Ocean Sci. Discuss., 8, 639–674, 2011
www.ocean-sci-discuss.net/8/639/2011/
doi:10.5194/osd-8-639-2011

Ocean Science Discussions

Silicon pool dynamics and biogenic silica export in the Southern Ocean, inferred from Si-isotopes

F. Fripiat[1,2], A.-J. Cavagna[3], F. Dehairs[3], S. Speich[4], L. André[1], and D. Cardinal[1,*]

[1]Section of Mineralogy and Petrography, Royal Museum for Central Africa, Tervuren, Belgium
[2]Department of Earth and Environmental Sciences, Université Libre de Bruxelles, Bruxelles, Belgium
[3]Analytical and Environmental Chemistry & Earth System Sciences, Vrije Universiteit Brussel, Brussels, Belgium
[4]Laboratoire de Physique des Océans, UMR 6523, IFREMER, CNRS, IRD, UBO, Plouzane, France
[*]now at: Laboratoire d'Océanographie et du Climat: Expérimentations et Approches Numériques, Université Pierre & Marie Curie, Paris, France

Received: 8 March 2011 – Accepted: 21 March 2011 – Published: 30 March 2011

Correspondence to: F. Fripiat (ffripiat@ulb.ac.be)

Published by Copernicus Publications on behalf of the European Geosciences Union.

Abstract

Water column silicon isotopic signatures (δ^{30}Si) of silicic acid ($Si(OH)_4$) in the Southern Ocean were measured along a meridional transect from South Africa (Subtropical Zone) down to 57° S (northern Weddell Gyre). These data are the first reported for a summer transect across the whole Antarctic Circumpolar Current (ACC). δ^{30}Si variations are large in the upper 1000 m, reflecting the effect of the silica pump superimposed upon meridional transfer across the ACC: the transport of Antarctic surface waters northward by a net Ekman drift and their convergence and mixing with warmer upper-ocean Si-depleted waters to the north. Using Si isotopic signatures, we determined different mixing interfaces between ACC water masses: the Antarctic Surface Water (AASW), the Antarctic Intermediate Water (AAIW), and the thermoclines in the low latitude areas. The residual silicic acid concentrations of end-members control the δ^{30}Si alteration of the mixing products. With the exception of AASW, all mixing interfaces have a highly Si-depleted mixed layer end-member. These processes deplete the silicic acid AASW concentration across the different interfaces northward without significantly changing the AASW δ^{30}Si. By comparing our new results with a previous study in the Australian sector we show that during the circumpolar transport of the ACC eastward, there is a slight but significant Si-isotopic lightening of the silicic acid pools from the Atlantic to the Australian sectors. This results either from the dissolution of biogenic silica in the deeper layers and/or from an isopycnal mixing with the deep water masses in the different oceanic basins: North Atlantic Deep Water in the Atlantic, and Indian Ocean deep water in the Indo-Australian sector. This eastward lightening is further transmitted to the subsurface waters, representing mixing interfaces between the surface and deeper layers.

Using the Si-isotopic constraint, we estimate for the Greenwich Meridian a net biogenic silica production which should be representative of the annual export, at 4.5 ± 1.1 and 1.5 ± 0.4 mol Si m^{-2} for the Antarctic Zone and Polar Front Zone, respectively, in agreement with previous estimations. The summertime Si-supply into the mixed layer

OSD
8, 639–674, 2011

via vertical mixing was also assessed at 1.5 ± 0.4 and 0.1 ± 0.5 mol Si m^{-2}, respectively.

1 Introduction

In the Southern Ocean deep nutrient-rich waters ascend into the surface layer and are returned equatorward as subsurface waters before the available pool of nitrogen is fully used by phytoplankton. This contrasts with silicon (in the form of silicic acid, $Si(OH)_4$), which is much more depleted by diatom growth and export along the same pathway (Sarmiento et al., 2004). The Southern Ocean redistributes nutrients at the global scale, thus representing the largest unused nutrient reservoir of the ocean interior, and bearing most of the potential to increase the efficiency of the marine carbon biological pump (Sigman et al., 2010). The large decoupling between nitrogen (N) and silicon (Si) impacts marine productivity at lower latitudes and is due to a complex interplay between (i) species effect difference in the silicification of diatom cells (Baines et al., 2010), (ii) iron and light limitation favouring heavily silicified diatoms (Takeda, 1998; Franck et al., 2003), (iii) the "silicate pump", which reflects the deeper remineralization of Si compared to N (Dugdale et al., 1995; Brzezinski et al., 2003a) and (iv) the structure of the microbial food web (Smetacek et al., 2004; Pondaven et al., 2007). The largest marine zonal silicic acid gradient across the Southern Ocean is thus controlled by surface water Si uptake by diatoms to form opaline cell walls (referred to as biogenic silica, $bSiO_2$), vertical mixing and subsequent intermediate water mass formation (Pondaven et al., 2000a; Brzezinski et al., 2001; Sarmiento et al., 2004, 2007). Deciphering the relative importance of these different processes which control the nutrient distribution in the Southern Ocean and how they affect nutrient export to the lower latitudes, is necessary to better constrain the role of the Southern Ocean in the global biogeochemical cycles at different timescales (past, present, and future) (Sarmiento et al., 2004; Sigman et al., 2010).

OSD
8, 639–674, 2011

The natural isotopic composition of silicon (δ^{30}Si) is a promising proxy to overcome both spatial and temporal variabilities in the marine silicon cycle since: (i) it integrates longer timescales and larger spatial scales compared to direct flux measurements (e.g. isotope dilution experiments; flux measurements using sediment traps, ...), (ii) it does not manipulate micro-organisms which can induce artefacts, and (iii) the different sensitivity of the mass and isotopic balances in marine systems means sources can be identified as well as the discrimination between different processes, e.g. $bSiO_2$ production (De La Rocha et al., 1997), $bSiO_2$ dissolution (Demarest et al., 2009), and mixing (Fripiat et al., 2011a). $Si(OH)_4$ uptake by diatoms leaves a clear imprint on the isotopic compositions of both $Si(OH)_4$ and $bSiO_2$. The fractionation factor ($^{30}\varepsilon = -1.1 \pm 0.4$‰) reported by De La Rocha et al. (1997) seems independent of temperature, species (De La Rocha et al., 1997), cell size (Cardinal et al., 2007) and appears relatively constant across contrasted hydrological environments including fresh water systems (Alleman et al., 2005). By compiling existing data sets Fripiat et al. (2011a) estimated an average $^{30}\varepsilon$ for the Antarctic Circumpolar Current (ACC) at -1.2 ± 0.2‰, a value indistinguishable from in vitro estimates. Biogenic silica dissolution preferentially releases light ^{28}Si with a fractionation factor of −0.55‰ (Demarest et al., 2009). This fractionation is counter to that occurring during Si-uptake, by about an absolute magnitude of half. By increasing the $bSiO_2$ dissolution:production (D:P) ratio, the overall fractionation factor would be dampened (Demarest et al., 2009). Currently spatial and seasonal coverage of δ^{30}Si measurements in the global ocean are limited and additional measurements, controlled experiments, and modelling efforts need to be done to better constrain the origin and fate of the isotopic composition, and to better assess modern and past distributions. Indeed, an important application of natural Si-isotopic variability is to track past silicon supply:consumption ratios by measuring δ^{30}Si of opal accumulating in sediments (De La Rocha et al., 1998; Brzezinski et al., 2002; Beucher et al., 2008).

In this study we present the first complete summer transect of $\delta^{30}Si_{Si(OH)_4}$ (surface to seafloor) in the different fronts and zones of the Antarctic Circumpolar Current (ACC)

OSD
8, 639–674, 2011

and its adjacent subsystems (the SubTropical Zone and the northern part of the Weddell Gyre). The results are discussed in terms of source, pathway, and fate of silicon across the different Southern Ocean water masses and the interaction of the latter with the water masses from other oceanic basins. Results are compared with a similar transect sampled in spring and located in the Australian sector of the Southern Ocean (CLIVAR-SR3; Cardinal et al., 2005). The isotopic constraints allow us to quantify the annual net $bSiO_2$ production and the vertical summertime Si-supply into the mixed layer, both in the Antarctic Zone and Polar Front Zone, using the approach described in Fripiat et al. (2011a). The surface Si-isotopic distribution is discussed further in detail in Fripiat et al. (2011b) while this study mainly focuses on the Si-isotopic distribution along the whole water column.

2 Materials and methods

The International Polar Year (IPY) BONUS-GoodHope (BGH) cruise covered a transect from Cape Town (South Africa) up to 58° S in the Southern Ocean roughly centred on the 0° meridian from 8 February to 8 March 2008, aboard the R/V *Marion Dufresne* (Fig. 1a). The general aim of BGH, a GEOTRACES-IPY endorsed project, is to understand the interactions between the physics and biogeochemistry in the Atlantic sector of the Southern Ocean and its exchanges with the Indo-Atlantic connection in the wake of the Agulhas system. Eleven stations were sampled for Si-isotopes, down complete water column profiles (~13 depths/station) and distributed across the different subsystems (Fig. 1a).

Seawater was collected using a CTD rosette equipped with 12 l Niskin bottles. Water samples (0.25 to 10 l) were immediately filtered on Nuclepore membranes (0.4 µm porosity) using Perspex filtration units under the pressure of filtered air. Filtered water samples for silicic acid analysis were stored in acid-cleaned polypropylene (PP) bottles at room temperature in the dark.

OSD
8, 639–674, 2011

Si-analyses

$Si(OH)_4$ concentrations were measured via a colorimetric method (Grasshoff et al., 1993) in the shore-based laboratory, on the same samples that were analyzed for Si-isotopic composition. Since $Si(OH)_4$ concentrations of surface and some subsurface waters at stations north of the Polar Front (PF) were too low (<10 µmol l^{-1}) to directly apply the Si purification procedure required for the Si-isotopic measurement (De La Rocha et al., 1996), a $Si(OH)_4$ preconcentration step was performed. The protocol used was adapted from the method described by Brzezinski et al. (2003b) and Reynolds et al. (2006) originally based on the MAGIC method (Karl and Tien, 1992). This consisted of a single- (or two-) step scavenging of $Si(OH)_4$ by a brucite ($Mg[OH]_2$) precipitate obtained by increasing the pH either with NaOH 1 µmol l^{-1} (20 ml l^{-1} seawater; Reynolds et al., 2006) or NH_4OH 13.5 µmol l^{-1} (6 ml l^{-1} seawater; Brzezinski et al., 2003b). The second scavenging was applied when the Si-recovery during the first step was incomplete. The precipitates were recovered by centrifugation and redissolved with HCl.

Silicon was co-precipitated with triethylamine molybdate (De La Rocha et al., 1996) with a minimum Si requirement of ~1.5 µmol. After combustion of the silicomolybdate precipitated in covered Pt crucibles at 1000 °C, the pure cristobalite phase was transferred to pre-cleaned PP vials. Dissolution of cristobalite was done in a dilute HF/HCl mixture as described in Cardinal et al. (2003). Isotopic measurements were carried out on a Nu Plasma MC-ICP-MS (ULB, Brussels) using Mg external doping in dry plasma mode following Abraham et al. (2008). The average precision and reproducibility of the measurements are ±0.15‰ (±2 sd) for $\delta^{30}Si$. The accuracy of the measurements is checked on a daily basis on secondary reference materials (e.g. Diatomite) whose Si-isotopic composition are well known, based on an inter-laboratory comparison exercise (Reynolds et al., 2007).

During the CLIVAR-SR3 cruise along the 145° E meridian (ACC; Australian sector; spring; Fig. 1b) $\delta^{29}Si$ was measured instead of $\delta^{30}Si$ (Cardinal et al., 2003, 2005),

OSD
8, 639–674, 2011

since the method used could not resolve interferences on ^{30}Si. To compare with the present BGH $\delta^{30}Si$ data, the CLIVAR SR-3 $\delta^{29}Si$ values were converted to $\delta^{30}Si$ values using the theoretical conversion factor of 1.96 calculated from the kinetic fractionation law (Young et al., 2002).

3 Results

In the mixed layer $\delta^{30}Si_{Si(OH)4}$ and $Si(OH)_4$ concentration displayed an inverse pattern with latitude (Table 1; Fig. 2a, b). ^{30}Si enrichment was associated with a decrease in $Si(OH)_4$ concentration from south to north, as also reported in earlier studies (Varela et al., 2004; Cardinal et al., 2005). This condition is mainly driven by the preferential uptake of ^{28}Si by diatoms (De La Rocha et al., 1997) along the northward advection of surface waters by Ekman pumping (Varela et al., 2004) followed by diatom export out of the mixed layer. The surface water Si-isotopic distribution and the control processes are discussed further in detail in Fripiat et al. (2011b), while the present study mainly focuses on the subsurface Si-isotopic distribution. This study reveals heavier summer surface $\delta^{30}Si_{Si(OH)_4}$ signatures in agreement with a larger seasonal $Si(OH)_4$ depletion (Fig. 2), compared with spring results (Cardinal et al., 2005), for two different ACC transects (Australian and Atlantic sectors, respectively, Fig. 1).

Most of the $\delta^{30}Si_{Si(OH)4}$ variation across the BONUS-Goodhope transect was limited to the upper 1000 m, with a clear north-south gradient showing heavier Si-isotopic values equatorward associated with a decrease in $[Si(OH)_4]$ (Figs. 2 and 3): mean $\delta^{30}Si_{Si(OH)_4}$ above 1000 m = 2.0 ± 0.5‰ vs. below 1000 m = 1.4 ± 0.1‰. Cardinal et al. (2005) observed a similar, though smaller, north-south gradient (Fig. 2d): mean $\delta^{30}Si_{Si(OH)_4}$ above 1000 m = 1.7 ± 0.3‰ vs. below 1000 m = 1.2 ± 0.1‰. Although the isotopic variation below 1000 m was small, there was still a slight lightening of the $\delta^{30}Si_{Si(OH)_4}$ with increasing $Si(OH)_4$ concentration (Fig. 3), as reported also by Cardinal et al. (2005) and Fripiat et al. (2011a). The Upper Circumpolar Deep Water (UCDW)

OSD
8, 639–674, 2011

had a slightly heavier $\delta^{30}Si_{Si(OH)_4}$ signature and a lower $Si(OH)_4$ concentration than Lower Circumpolar Deep Water (LCDW) and Antarctic Bottom Water (AABW; Table 2).

In the following discussion, the different water masses (Table 2) are defined by their potential temperature, salinity, and O_2 properties: UCDW (oxygen minimum), LCDW (depth salinity maximum), Antarctic Intermediate Water (AAIW; subsurface salinity minimum), Winter Water (WW, subsurface temperature minimum), SAZ-STZ thermoclines (between AAIW and the mixed layer, ML), and AABW (bottom increases in O_2 content, decreases in temperature and salinity).

4 Discussion

4.1 General considerations

In the following discussion, we will follow the silicon pathway and the transformations encountered along the meridional as well as the circumpolar circulations of ACC. The ACC represents the largest mass transport of all ocean currents, a slab of water more than 2000 m thick moving eastward (Tomczak and Godfrey, 2001), but mainly centered in several jets along frontal systems: the inner ACC fronts (Sokolov and Rintoul, 2009); SubAntarctic Front, Antarctic Polar Front, Southern ACC Front. The ACC fronts represent almost impermeable barriers delimiting zones with relatively constant hydrological and biogeochemical properties (Sokolov and Rintoul, 2007). Cross frontal exchanges do occur locally, associated with sharp topographic features. This wind-driven meridional circulation is characterised from south to north by: (1) the shoaling of deeper isopycnal surfaces (UCDW and LCDW) in the Southern ACC near the Antarctic divergence (Pollard et al., 2002, 2006), (2) part of the upwelled CDW losing buoyancy near Antarctica to form AABW (Orsi et al., 1999) and the remaining gaining buoyancy and being advected northward (Antarctic Surface Water, AASW) via Ekman pumping (Sloyan and Rintoul, 2001; Pollard et al., 2002), (3) the subsequent formation of intermediate water masses taking place (AAIW, and SubAntarctic Mode Water, SAMW),

OSD
8, 639–674, 2011

spreading and deepening northward of the PF (Sarmiento et al., 2004). The latitudinal δ^{30}Si variation in the water column follows this meridional circulation (Fig. 2).

4.2 Isotopic constraints on the silicic acid leakage from the Southern Ocean to the low latitude areas

4.2.1 Southern ACC

We define the southern ACC as the area south of the Polar Front where isopycnal surfaces shoal and UCDW and LCDW upwell near the surface. From Fig. 4, it is apparent that the subsurface waters (WW and UCDW) in the southern ACC are mixing interfaces between LCDW and AZ mixed layers. Indeed, both AZ-PF Winter Water (WW) and UCDW fit well on a mixing line with the AZ-PF mixed layer and the LCDW as end-members, in agreement with our observations for the Indian sector of the Southern Ocean (Fripiat et al., 2011a). The UCDW and AZ-PF mixed layer generate a homogeneous deep winter mixed layer at the onset of the winter convective mixing known as the Antarctic Surface Water (AASW; Park et al., 1998). Due to surface warming in the summer, the Antarctic Surface Water becomes stratified, with the ML above and the WW below, with the latter still carrying the original AASW characteristics (Pondaven et al., 2000a; Altabet and François, 2001; Fripiat et al., 2011a; Cavagna et al., 2011).

Using the mixing line with the mean UCDW and AZ-PF ML values (Fig. 4; Table 2), we can estimate the mean UCDW Si mass fraction contribution to AASW (represented by the mean of the AZ-PF WW) is 0.85 in the AZ. This value is close from the value reported for the HNLC area east of the Kerguelen plateau, at 0.78 (Fripiat et al., 2011a). Integrating the WW $Si(OH)_4$ concentration over the water layer between the surface and bottom waters of the WW (i.e. AASW which represents 300 ± 50 m) and multiplying that amount with the UCDW contribution, UCDW contributes 12.3 ± 2.0 mol Si m^{-2} to AASW. Standard errors for the different water mass balance estimations were obtained from Montecarlo simulations (Normal distribution, $n = 1000$). The 100 ± 25 m deep summer ML will thus inherit $(100/300) \cdot (12.3 \pm 2.0 \text{ mol Si m}^{-2})$ or 4.5 ± 1.1 mol Si m^{-2}

OSD
8, 639–674, 2011

which becomes available at the start of the growth season. Assuming that steady state conditions apply (i.e. the supply equals the export at the annual scale), the effective annual net $bSiO_2$ production should be equal to the annual vertical UCDW Si-supply of 4.5 ± 1.1 mol Si m^{-2}, which is again indistinguishable with our previous Indian sector estimation of 4.0 ± 0.7 mol Si m^{-2} (Fripiat et al., 2011a). This value exceeds the seasonal depletion, 3.0 ± 0.8 mol Si m^{-2} yr^{-1}, as estimated from a simple mixed layer mass balance (i.e. difference between WW and ML $Si(OH)_4$ concentration). This discrepancy highlights that some 1.5 ± 0.4 mol Si m^{-2} yr^{-1} are being supplied to the mixed layer during the stratification period, a flux similar to that observed for the Indian sector (Fripiat et al., 2011a). Our estimated annual net $bSiO_2$ production values slightly exceeds the range of published net $bSiO_2$ production values for the AZ (2.4 to 3.3 mol Si m^{-2} yr^{-1}; Pondaven et al., 2000a; Nelson et al., 2002; Pollard et al., 2006). Using an inverse modeling approach for nutrient distributions, Jin et al. (2006) estimated opal export out of the euphotic layer in the Southern Ocean in the range of 1 to 9 mol Si m^{-2} yr^{-1}, which encompasses our estimate of net $bSiO_2$ production. Integrating our estimation over the whole AZ area (14.10^6 km^2, JGOFS synthesis report, 2001), the net $bSiO_2$ production is 63 ± 15 Tmol Si yr^{-1} including 21 ± 6 Tmol Si yr^{-1} coming from the summertime silicon supply. Taking into account a global net biogenic silica production at 171 ± 35 Tmol Si yr^{-1} (mean from Nelson et al., 1995; Usbeck, 1999; Heinze et al., 2003; Jin et al., 2006), the net biogenic silica production in the AZ contributes at 33 ± 12%.

4.2.2 Northern ACC and STZ

Here, the northern ACC is defined as the area north to the PF and we include in this study the STZ, although the STZ is not part of ACC. The subsurface waters in the PFZ (halocline) fall on a mixing line between the PF-AZ AASW and PFZ-PF ML (Fig. 5a). The subsurface layers in the PFZ could be a precursor of AAIW, spreading and deepening northwards through mesoscale frontal circulation (e.g. meanders

OSD
8, 639–674, 2011

and eddies; Speich et al., 2011, this issue). In this sector of the Southern Ocean, AAIW-type waters were observed north of the SAF (salinity minimum layer, ~500 to 1000 m) but mainly of an Indian Ocean origin (Reid, 2003). Nevertheless, the AAIW north of the SAF is not significantly different from the PFZ subsurface waters in terms of Si-properties (Fig. 5a). This could be explained by similar formation dynamics such as AASW mixing with highly Si-depleted mixed layers northward. Whereas the involvement of AASW to form AAIW is well established, the exact mechanisms are still unclear (Molinelli, 1981; England et al., 1993; Sloyan and Rintoul, 2001; Morrow et al., 2004). Tomczak and Godfrey (2001) concluded that both circumpolar cross-frontal mixing and PFZ local deep convective mixing plays a role, in agreement with our data.

The mean AAIW does not fall on the mixing line with the mean AZ-PF AASW (= AZ-PF WW) and PFZ ML as end-members (Fig. 4). This results from the fact that the mean AZ-PF AASW is not representative of the AASW flowing into the PFZ via cross frontal exchanges. In contrast, taking strictly the AASW (= PF WW) Si-properties at the PF as end-member, the mean AAIW falls on the mixing line with PFZ-ML and therefore PF AASW are better representative of a cross frontal exchange end-member. As was done for the AZ, we estimate here that the AASW Si mass fraction contribution to AAIW is 0.96. This high value highlights that almost all the Si in the AAIW originates from the AASW layer with only a very low residual Si-contribution from the summer PFZ mixed layers. Assuming a system in steady state, as described above for the AZ, the annual AASW Si-supply into the AAIW equals the net $bSiO_2$ production, 1.5 ± 0.4 mol Si m^{-2} yr^{-1}. This estimation was done by integrating AAIW over 750 ± 250 m and the ML integrating depth at 80 ± 20 m following T-S water column properties during BGH. The seasonal Si-depletion (from the difference between AAIW and PFZ ML $Si(OH)_4$ concentrations) is estimated to be 1.4 ± 0.3 mol Si m^{-2} yr^{-1}. This value is close to the net $bSiO_2$ production estimate implying large uncertainties in the summertime Si-supply, 0.1 ± 0.5 mol Si m^{-2} yr^{-1}. Fripiat et al. (2010), compiling Si-uptake and $bSiO_2$ dissolution from tracer incubation experiments, noted that the mean net $bSiO_2$ production in the PFZ was 1.2 mol Si m^{-2} yr^{-1}, close to our estimate for

OSD
8, 639–674, 2011

the present study. Integrating our estimation, 1.5 ± 0.4 mol Si m^{-2} yr^{-1}, over the whole PFZ area (3.10^6 km^2, JGOFS synthesis report, 2001), the net $bSiO_2$ production for the whole PFZ is 5 ± 1 Tmol Si m^{-2} yr^{-1}, 3 ± 1% of the global net biogenic silica production (Nelson et al., 1995; Usbeck, 1999; Heinze et al., 2003; Jin et al., 2006). Diatom activity in the PFZ removes subsequently a slight fraction of the Si entering in the PFZ. The lower $Si(OH)_4$ concentration of AAIW layer results mainly from a highly $Si(OH)_4$ depleted surface water at PF and in PFZ decreasing the $Si(OH)_4$ content of the resulting mixing product (AAIW) without significant change in δ^{30}Si (Figs. 4, 5, 6).

Analysing the NO_3-isotopic distribution, Sigman et al. (1999) suggested that the main source for NO_3 in the PFZ was AASW advected northwards by Ekman drift, in agreement with our data. They report the AAIW to be only slightly different from AASW in terms of NO_3 concentration and isotopic composition, which contrasts with our observations for Si, especially regarding $Si(OH)_4$ concentration, which is significantly lower in AAIW than in AASW. The large decoupling between the seasonal depletion of $Si(OH)_4$ and NO_3 in the mixed layer could explain the difference between this study and Sigman et al. (1999) regarding the degree of AASW alteration during formation of AAIW. $[NO_3]$ is still high at the PF and PFZ (30 to 20 µmol l^{-1}) compared to $[Si(OH)_4]$ (<5 µmol l^{-1}), while Si and N contents of PF WW are both ~35 µmol l^{-1}. As a result, NO_3-biogeochemical properties of AAIW appear closer to those for AASW, leading Sigman et al. (1999) to conclude that unaltered AASW is the main source for the AAIW nitrate pool.

The subsurface waters in SAZ and STZ are characterized by a thermocline between the mixed layer and the AAIW below (salinity minimum layer). Despite the fact that values fall slightly below the mixing line, the Si characteristics in Fig. 5b clearly identify the thermocline in the SAZ and STZ as being a mixing interface between AAIW and the SAZ-STZ ML. The slight offset could be explained by the fact that the entire subtropical region just north of our representative SAZ station (S2; Fig. 1a) is impacted by the Agulhas Current. This is the western boundary current flowing southward along the Southern Eastern Africa continental slope before retroflecting eastward and forming

OSD
8, 639–674, 2011

intense anticyclonic eddies (Agulhas rings), constituting the STF in the Indo-Atlantic sector and potentially crossing the STF into the SAZ region (Decausse et al., 2011). These rings supply into this region Indian central waters and AAIW of Indian origin. Since we did not sample the variety of the mixing end-members, it is not possible to estimate the net $bSiO_2$ production and the summertime Si-supply as done for the PFZ and the AZ.

The spreading and deepening northward of the Southern Ocean water masses (Sub-Antarctic Mode Water (SAMW), which was observed respectively across CLIVAR-SR3 but not across BGH; and AAIW) is propagated towards the Equatorial Pacific, as clearly seen from their similitude with the Si isotopic composition of subsurface waters in the Equatorial Pacific (Beucher et al., 2008, Fig. 7). This indicates AAIW – SAMW waters are the main Si-suppliers to the surface waters at lower latitudes in agreement with Sarmiento et al. (2004). The North Pacific Ocean is one of the main exceptions to the worldwide dominance of the AAIW-SAMW as the origin of Si supply to the surface. In this area, the thermocline silicic acid pool seems to be fed by the North Pacific Intermediate water (NPIW; Sarmiento et al., 2004), bearing lighter δ^{30}Si values (De La Rocha et al., 2000; Reynolds et al., 2006; Fig. 7). Strong vertical mixing, supplying silicic acid from Si-rich NPDW, is an important contributor to the processes that determine the biogeochemical properties of NPIW (Sarmiento and Gruber, 2006), including lighter δ^{30}Si values (De La Rocha et al., 2000; Reynolds et al., 2006).

4.2.3 Paleoceanographic implications

The fact that the mesopelagic layers (~100–1000 m) with their Si content and isotopic characteristics are the source region for Si to most of the surface waters, has significant implications for the paleoceanographic interpretation of the δ^{30}Si records preserved in the sediments. Different ACC mixing interfaces have been identified: AASW, AAIW, both characterizing the halocline, and the thermocline water northwards. The residual silicic acid concentrations of the end-members control the δ^{30}Si alteration of the mixing products. Except for AASW, all the mixing interfaces have a highly Si-depleted

OSD
8, 639–674, 2011

mixed layer as end-member. As a result, the silicic acid AASW concentration is diluted across the different interfaces without significantly changing the AASW δ^{30}Si signature (Fig. 6). Si-utilization in the northern ACC and at lower latitudes will thus yield a similar surface water δ^{30}Si range than in the southern ACC but with a lower silicic acid concentration (Figs. 6, 7). The North Pacific Ocean has significantly lighter δ^{30}Si values and consequently, for similar levels of Si-utilization, the δ^{30}Si of the resulting surface water will be lighter. From the palaeoceanographic perspective, the mesopelagic variation in δ^{30}Si induces a complexity since glacial circulation and hydrology is expected to be different from today (Toggweiler et al., 2006; Watson et al., 2006). It is probable that different oceanic circulations altered the Si-properties of water masses and subsequently the δ^{30}Si of the source regions feeding surface waters. δ^{30}Si in the subsurface varies between +1.3 to +2.0‰ (Fig. 2b, d), a range which is significant with regard to the isotopic difference observed for Southern Ocean sediments between glacial/interglacial periods (~+0.2 to +1.5‰ in the AZ, De La Rocha et al., 1998; Brzezinski et al., 2002, and ~+1 to +2‰ in the SAZ, Beucher et al., 2007). These dynamic effects must be assessed through, for example, a process-oriented modelling effort.

4.3 Inter-oceanic leakage of Si-isotopes.

In deep waters along the pathway of the global ocean overturning circulation, silicic acid concentration increases in the North Atlantic Deep Waters (NADW) along their pathway in the Atlantic until reaching the North Pacific and North Indian as the NPDW and the Indian Ocean Deep Water (IODW) (Fig. 8a). Progressive accumulation of dissolved Si from $bSiO_2$ dissolution is the main driver of this condition (Sarmiento et al., 2004, 2007) as is the case also for the other macronutrients. The distribution of the δ^{30}Si of silicic acid decreases from ~+1.4‰ in NADW to ~+0.6‰ in NPDW (Fig. 8a; De La Rocha et al., 2000; Reynolds et al., 2006). Progressive accumulation of silicic acid from $bSiO_2$ dissolution could sustain this change in isotopic signature (De La Rocha et al., 2000; Reynolds, 2009) as observed also for $\delta^{13}C_{DIC}$ due to the

OSD
8, 639–674, 2011

remineralization of organic matter (Kroopnick, 1985). The lack of a δ^{30}Si gradient along the path of the NADW to the Circumpolar Deep Waters (CDW, represented here CDW and UCDW along the BGH transect) probably results from the fact that silicic acid is almost completely consumed in most of the Atlantic Ocean surface waters (Conkright et al., 2002). Therefore, the integrated δ^{30}Si of sinking biogenic silica converges to the one of the source, i.e. silicic acid supply, so that the δ^{30}Si of the $bSiO_2$ rain-out from the surface is similar to that of subsurface silicic acid (initially mostly AAIW) ultimately sinking to form NADW in the North Atlantic (Sarmiento et al., 2004; Reynolds, 2009). The subsequent Si-isotopic lightening from the CDW to the NPDW (Fig. 8a) can be attributed to the dissolution of settling diatoms in areas where silicic acid is only partly used. Consequently it should integrate δ^{30}Si signatures significantly lighter that the source, as is the case for the Southern Ocean and North Pacific (Pondaven et al., 2000b; Brzezinski et al., 2001). Contrasting with Reynolds (2009) who reports, based on a modelling approach, that the Si isotopic gradient is centered in the Southern Ocean deep waters, the measured isotopic gradient in deep waters (~1.0‰) is in fact sharper along the deep Pacific basins, while the isotopic shift observed along the ACC pathway shows only a slight, though significant (ANOVA, p value < 0.01) ^{30}Si depletion of ~0.2‰ (Fig. 8b).

Toggweiler et al. (2006) partitioned the global ocean's overturning circulation in two components, the northern and southern domains which occupy distinct domains in the ocean's interior as detailed in the following. In the modern ocean these waters mix together in the ocean's interior to form CDW, which comes up to the surface along the southern flank of the ACC. The mid depth northern domain is the domain of North Atlantic Deep Water (NADW) presenting lower $Si(OH)_4$ concentration and heavier δ^{30}Si (Fig. 8a). The lower ventilated southern domain is the domain of the deep and bottom water, as AABW, IODW, and NPDW, with higher $Si(OH)_4$ concentration and lighter δ^{30}Si (Fig. 8a). This process should explain partly the isotopic gradient through isopycnal mixing from the Atlantic sector where NADW enters the Southern Ocean to the Australian sector where waters are potentially already significantly affected by the mixing

OSD
8, 639–674, 2011

with the IODW (Reid, 2003), probably bearing a lighter Si-isotopic composition as in the NPDW. Moreover the partitioning of the global ocean's overturning circulation in two components (Toggweiler et al., 2006) could act as a positive feedback for the isotopic expression of biogenic silica dissolution effect in the Pacific Ocean since silicic acid is trapped in the Pacific Ocean presenting lower ventilation (Sarmiento et al., 2007).

An unexpected feature is the much heavier isotopic composition in the eastern Pacific, Equatorial and Cascadia basin (Beucher et al., 2008) compared to western northern Pacific (Fig. 8a; De La Rocha et al., 2000; Reynolds, 2009). Clearly more data for the deep Pacific and Indian Oceans are required in order to resolve the deep Si-isotope distribution pattern and to identify the mechanisms driving it.

The isotopic gradient in deep waters along the global overturning circulation seems to be also expressed in the δ^{30}Si values in the ACC subsurface waters between the Atlantic and the Australian sectors. Indeed, WW which is representative of winter AASW (Sect. 4.3) also displays a Si-isotopic lightening from the Atlantic to the Australian sector (Fig. 8c; regression lines, are significantly different, ANOVA, p value < 0.01, both, for slope and y-intercept) as observed for the AAIW, the SAMW, and the SAZ-STZ thermoclines (Fig. 8d; ANOVA, p value < 0.01). If these trends are confirmed by a larger data set, they are to be taken into account when interpreting sedimentary archives and request the use of an appropriate correction factor. There is also need to further verify whether the observed trend in isotopic composition is confirmed along the ACC pathway in the Pacific.

5 Conclusions

We report the first summer-season isotopic compositions of silicic acid (δ^{30}Si) across the whole ACC and adjacent subsystems, the SubTropical Zone and the Weddell Gyre, for the full-depth water column in the Atlantic sector.

In a similar way as reported in Fripiat et al. (2011a), we used the Si-isotopic constraint to assess (1) the net $bSiO_2$ production and (2) the summertime Si-supply into the mixed

OSD
8, 639–674, 2011

layer: (1) 4.1 ± 1.0 and 1.5 ± 0.4 mol Si m^{-2} and (2) 1.1 ± 0.3 and 0.1 ± 0.5 mol Si m^{-2}, respectively for the mean Antarctic Zone and Polar Front Zone. The net biogenic silica production is in the range of previous estimates. Integrating our estimation over the whole AZ and PFZ area (JGOFS synthesis report, 2001), the net $bSiO_2$ production contributes at 33 ± 12 and 3 ± 1% to the global net biogenic silica production (171 ± 35 Tmol Si yr^{-1}; Nelson et al., 1995; Usbeck, 1999; Heinze et al., 2003; Jin et al., 2006).

δ^{30}Si in the subsurface waters is mainly controlled by mixing processes transmitting the isotopic imprint resulting from surface water Si-uptake down to depth. Different mixing interfaces have been determined: the Antarctic Surface Water, the Antarctic Intermediate Water, and the low latitude thermoclines. The level of Si-depletion seems to be an important factor controlling the alteration of δ^{30}Si in the mixing interface. Indeed, a highly Si-depleted water mass dilutes the silicic acid concentration of the mixing product without significantly affecting δ^{30}Si. Except for the AASW which is the ultimate source for the subsurface waters in the ACC, each mixing interface has a highly depleted mixed layer as an end-member. Overall the AASW silicic acid concentration decreases strongly across the different mixing interfaces northward, keeping the initial AASW δ^{30}Si signature. Consequently, almost all surface water in the modern ocean is characterised by a similar range in δ^{30}Si, though silicic acid concentration levels differ.

The ocean hydrology and circulation is expected to be different between glacial/interglacial periods. Modification of the ocean's circulation could significantly affect the δ^{30}Si of subsurface waters affecting biogenic silica production in surface waters. Through a process-oriented modelling effort, this mixing induced variability in δ^{30}Si has to be better constrained for the proper use of this proxy in paleoceanography.

A progressive lightening of δ^{30}Si across the water masses is observed along the eastward ACC transport between the Atlantic (this study) and the Australian sector (Cardinal et al., 2005). This probably results from: (1) the progressive accumulation of Si from dissolving biogenic silica along the eastward ACC transport and (2) isopycnal mixing between deep water masses in each of the oceanic basins. Should this

OSD
8, 639–674, 2011

ACC trend be further confirmed from new Pacific ACC transects, the isotopic effect would then need to be corrected, for proper interpretation of the biogenic silica δ^{30}Si signatures preserved in the sediments.

Acknowledgements. Our warm thanks go to the officers and crew of the R/V *Marion Dufresne* during the BONUS-Goodhope program. We are also grateful to J. De Jong and N. Mattielli for the management of the MC-ICP-MS laboratory at ULB and to L. Monin and N. Dahkani (RMCA) for their help in sample processing and to Virginia Panizzo (ULB) for improvement of English. This work was conducted within the BELCANTO III network (contracts SD/CA/03A of SPSDIII, Support Plan for Sustainable Development) funded by BELSPO, the Belgian Science Policy. Luc André thanks the FNRS for its financial support (FRFC project 2.4512.00). François Fripiat is funded by the "Fonds National de la Recherche Scientifique" (FNRS, Belgium).

References

Abraham, K., Opfergelt, S., Fripiat, F., Cavagna, A.-J., de Jong, J. T. M., Foley, S. F., André, L., and Cardinal, D.: δ^{30}Si and δ^{29}Si determinations on USGS BHVO-1 and BHVO-2 reference materials with a new configuration on a Nu Plasma Multi-Collector ICP-MS, Geostand. Geoanal. Res., 32(2), 193–202, 2008.

Alleman, L., Cardinal, D., Cocquyt, C., Plisnier, P. D., Descy, J.-P., Kimirei, I., Sinyinza, D., and André, L.: Silicon isotopic fractionation in Lake Tanganyika and its main tributaries, J. Great Lakes Res., 31, 509–519, 2005.

Altabet, M. A. and Francois, R.: Nitrogen isotope biogeochemistry of the Antarctic Polar Frontal Zone at 170° W, Deep-Sea Res. Pt. II, 48, 4247–4273, 2001.

Aumont, O., Maier-Reimer, E., Blain, S., and Monfray, P.: An ecosystem model of the global ocean including Fe, Si, P co-limitation, Global Biogeochem. Cy., 17(2), 1060, doi:10.1029/2001GB001745, 2003.

Baines, S. B., Twining, B. S., Brzezinski, M. A., Nelson, D. M., and Fisher, N. S.: Causes and biogeochemical implications of regional differences in silicification of marine diatoms, Global Biogeochem. Cy., 24, GB4031, doi:10.1029/2010GB003856, 2010.

Beucher, C. P., Brzezinski, M. A., and Crosta, X.: Silicic acid dynamics in the glacial

OSD

8, 639–674, 2011

sub-Antarctic: Implications for the silicic acid leakage hypothesis, Global Biogeochem. Cy., 21, GB3015, doi:10.1029/2006GB002746, 2007.
Beucher, C. P., Brzezinski, M. A., and Jones, J. L.: Sources and biological fractionation of silicon isotopes in the Eastern Equatorial Pacific, Geochim. Cosmochim. Ac., 72, 3063–3073, 2008.
Brzezinski, M. A., Nelson, D. M, Franck, V. M., and Sigmon, D. E.: Silicon dynamics within an intense open-ocean diatom bloom in the Pacific sector of the Southern Ocean, Deep-Sea Res. Pt. II, 48, 3997–4018, 2001.
Brzezinski, M. A., Pride, C. J., Franck, V. M., Sigman, D. M., Sarmiento, J. L., Matsumoto, K., Gruber, N., Rau, G. H., and Coale, K. H.: A switch from $Si(OH)_4$ to NO_3^- depletion in the glacial Southern Ocean, Geophys. Res. Lett. 29(12), 1564, doi:10.1029/2001GL014349, 2002.
Brzezinski, M. A., Dickson, M.-L., Nelson, D. M., and Sambrotto, R.: Ratios of Si, C and N uptake by microplankton in the Southern Ocean, Deep Sea Res. Pt. II, 50, 619–633, 2003a.
Brzezinski, M. A., Jones, J. L., Bidle, K. D, and Azam, F.: The balance between silica production and silica dissolution in the sea: Insights from Monteray Bay, California, applied to the global data set, Limnol. Oceanogr. 48(5), 1846–1854, 2003b.
Cardinal, D., Alleman, L. Y., de Jong, J., Ziegler, K., and André, L.: Isotopic composition of silicon measured by multicollector plasma source mass spectrometry in dry plasma mode, J. Anal. Atom. Spectrom., 18, 213–218, 2003.
Cardinal, D., Alleman, L. Y., Dehairs, F., Savoye, N., Trull, T. W., and André, L.: Relevance of silicon isotopes to Si-nutrient utilization and Si-source assessment in Antarctic waters, Global Biogeochem. Cy., 19, GB2007, doi:10.1029/2004GB002364, 2005.
Cardinal, D., Savoye, N., Trull, T. W., Dehairs, F., Kopczynska, E. E., Fripiat, F., Tison, J.-L., and André, L.: Silicon isotopes in spring Southern Ocean diatoms: large zonal changes despite homogeneity among size fractions, Mar. Chem., 106, 46–62, 2007.
Cavagna, A.-J., Fripiat, F., Dehairs, F., Wolf-Gladrow, D., Cisewski, B., Savoye, N., André, L., and Cardinal, D.: Silicon uptake and supply during a Southern Ocean iron fertilization experiment (EIFEX) tracked by Si isotopes, Limnol. Oceanogr., 56(1), 147–160, 2011.
Conkright, M. E., Locarnini, R. A., Garcia, H. E., O'Brien, T. D., Boyer, T. P., Stephens, C., and Antonov, J. I.: World Ocean Atlas 2001; Ojective Anlyses, Data Statistics, and Figures, CD-ROM Documentation, Natl. Oceanogr. Data Cent., Silver Spring, Md, 2002.
De La Rocha, C. L., Brzezinski, M. A., and DeNiro, M. J.: Purificaiton recovery and laser-driven fluorination of silicon from dissolved and particulate silica for the measurement of natural

OSD
8, 639–674, 2011

stable isotope abundances, Anal. Chem., 68, 3746–3750, 1996.
De La Rocha, C. L., Brzezinski, M. A., and DeNiro, M. J.: Fractionation of silicon isotopes by marine diatoms during biogenic silica formation, Geochim. Cosmochim. Ac., 61(23), 5051–5056, 1997.
De La Rocha, C. L., Brzezinski, M. A., and DeNiro, M. J.: Silicon-isotope composition of diatoms as an indicator of past oceanic change, Nature, 395, 680–683, 1998.
Demarest, M. S., Brzezinski, M. A., and Beucher, C. P.: Fractionation of silicon isotopes during biogenic silica dissolution, Geochim. Cosmochim. Ac., 73, 5572–5583, doi:10.1016/j.gca.2009.06.019, 2009.
Dencausse, G., Arhan, M., and Speich, S.: Is there a continuous Subtropical Front south of Africa?, J. Geophys. Res. 116, C02027, doi:10.1029/2010JC006587, 2011.
Dugdale, R. C., Wilkerson, F. P., and Minas, H. J: The role of a silicate pump in driving new production, Deep-Sea Res. Pt. I, 42(5), 697–719, 1995.
England, M. H., Godfrey, J. S., Hirst, A. C., and Tomczak, M.: The mechanism for Antarctic Intermediate Water renewal in a world Ocean Model, J. Phys. Oceanogr., 23, 1553–1560, 1993.
Franck, V. M., Bruland, K. W., Hutchins, D. A., and Brzezinski, M. A.: Iron and zinc effects on silicic acid and nitrate uptake kinetics in three high-nutrient, low-chlorophyll (HNLC) regions, Mar. Ecol.-Prog. Ser., 252, 15–33, 2003.
Fripiat, F., Leblanc, K., Elskens, M., Cavagna, A.-J., Armand, L., André, L., Dehairs, F., and Cardinal, D.: Summer efficient silicon loop across the Polar Front and SubAntarctic Zones despite contrasted diatom Si-affinity, Mar. Ecol.-Prog. Ser., submitted, 2010.
Fripiat, F., Cavagna, A.-J., Savoye, N., Dehairs, F., André, L., and Cardinal, D.: Isotopic constraints on the Si-biogeochemical cycle of the Antarctic Zone in the Kerguelen area (KEOPS), Mar. Chem., 123, 11–22, 2011a.
Fripiat, F., Cavagna, A.-J., Dehairs, F., André, L., and Cardinal, D.: Si-isotopic composition of suspended biogenic silica in the Southern Ocean, Biogeosciences Discuss., in preparation, 2011b.
Grasshof, K., Erhardt, M., and Kremling, K.: Methods of seawater analysis, 2nd edn., Verlag Chemie, Weinheim, 1983.
Heinze, C., Hupe, A., Maier-Reimer, E., Dittert, N., and Ragueneau, O.: Sensitivityof the marine biospheric Si-cycle for biogeochemical parameter variations, Global Biogeochem. Cy., 17(3), 1086, doi:10.1029/2002GB001943, 2003.

OSD
8, 639–674, 2011

Jin, X., Gruber, N., Dunne, J. P., Sarmiento, J. L., and Amstrong, R. A.: Diagnosing the contribution of phytoplankton functional groups to the production and export of particulate organic carbon, CaCO3, and opal from global nutrient and alkalinity distributions, Global Biogeochem. Cy., 20, GB2015, doi:10.1029/2005GB002532, 2006.

Karl, D. M. and Tien, G.: MAGIC: a sensitive and precise method for measuring dissolved phosphorus in aquatic environments, Limnol. Oceanogr., 37(1), 105–116, 1992.

Kroopnick, P. M.: The distribution of ^{13}C of TCO2 in the world oceans, Deep-Sea Res. A, 32, 57–84, 1985.

Lutjeharms, J. and van Ballegooyen, R.: The retloflection of the Agulhas Current, J. Phys. Oceanogr., 18, 761–774, 1988.

Molinelli, E. T.: The Antarctic influence on Antarctic Intermediate Water, J. Mar. Res., 39, 267–293, 1981.

Morrow, R. A., Coleman, R., Church, J. A., and Chelton, D. B.: Surface eddy momentum flux and velocity variances in the Southern Ocean from geosat altimetry, J. Phys. Oceangr., 24, 2050–2071, 2004.

Nelson, D. M., Tréguer, P., Brzezinski, M. A., Leynaert, A., and Quéguiner, B.: Production and dissolution of biogenic silica in the ocean: revised global estimates comparison with regional data and relationship to biogenic sedimentation, Global Bigeochem. Cy., 9(3), 359–372, 1995.

Nelson, D. M., Anderson, R. F., Barber, R. T., Brzezinski, M. A., Buesseler, K. O., Chase, Z., Collier, R. W., Dickson, M.-L., François, R., Hiscock, M. R., Honjo, S., Marra, J., Martin, W. R., Sambrotto, R. J., Sayles, F. L., and Sigmon, D. E.: Vertical budgets for organic carbon and biogenic silica in the Pacific sector of the Southern Ocean, 1996–1998, Deep Sea Res. Pt. II, 49, 1645–1674, 2002.

Orsi, A. H., Johnson, G. C., and Bullister, J. L.: Circulation, mixing, and production of Antarctic Bottom Water, Prog. Oceanogr., 43, 55–109, 1999.

Park, Y.-H., Charriaud, E., and Fieux, M.: Thermohaline structure of the Antarctic Surface Water/Winter Water in the Indian sector of the Southern Ocean, J. Marine Syst., 17, 5–23, 1998.

Pollard, R. T., Lucas, M. I., and Read, J. F.: Physical controls on biogeochemical zonation in the Southern Ocean, Deep-Sea Res., 49, 3289–3305, 2002.

Pollard, R. T., Tréguer, P., and Read, J.: Quantifying nutrient supply to the Southern Ocean, J. Geophys. Res., 111, C05011, doi:10.1029/2005JC003076, 2006.

OSD
8, 639–674, 2011

Pondaven, P., Ragueneau, O., Tréguer, P., Hauvespre, A., Dezileau, L., and Reyss, J. L.: Resolving the opal paradoxe in the Southern Ocean, Nature, 405, 168–172, 2000a.
Pondaven, P., Ruiz-Pino, D., Fravalo, C., Tréguer, P., and Jeandel, C.: Interannual variability of Si and N cycles at the time-series station KERFIX between 1990 and 1995 – a 1-D modelling study, Deep-Sea Res. Pt. I, 47, 223–257, 2000b.
Pondaven, P., Gallinari, M., Chollet, S., Bucciarelli, E., Sarthou, G., Schultes, S., and Jean, F.: Grazing-induced changes in cell wall silicification in a marine diatoms, Protist, 158, 21–28, 2007.
Reid, J. L.: On the total geostrophic circulation of the Indian Ocean: flow patterns, tracers, and transports, Prog. Oceanogr., 56, 137–186, 2003.
Reynolds, B. C., Frank, M., and Halliday, A. N.: Silicon isotope fractionation during nutrient utilization in the North Pacific, Earth Planet. Sc. Lett., 244, 431–443, 2006.
Reynolds, B. C., Aggarwal, J., André, L., Baxter, D., Beucher, C., Brzezinski, M. A., Engström, E., Georg, R. B., Land, M., Leng, M. J., Opfergelt, S., Rodushkin, I., Sloane, H. J., van den Boorn, H. J. M., Vroon, P. Z., and Cardinal, D.: An inter-laboratory comparison of Si isotope reference materials, J. Anal. Atom. Spectrom., 22, 561–568, doi:10.1039/b616755a, 2007.
Reynolds, B. C.: Modeling the modern marine δ^{30}Si distribution, Global Biogeochem. Cy., 23, GB2015, doi:10.1029/2008GB003266, 2009.
Sarmiento, J. L. and Gruber, N.: Ocean biogeochemical dynamics, Princeton University Press, Princeton NJ, 2006.
Sarmiento, J. L., Gruber, N., Brzezinski, M. A., and Dunne, J. P.: High-latitude controls of thermocline nutrients and low latitude biological productivity, Nature, 427, 56–60, 2004.
Sarmiento, J. L., Simeon, J., Gnanadesikan, A., Gruber, N., Key, R. M., and Schlitzer, R.: Deep ocean biogeochemistry of silicic acid and nitrate, Global Biogeochem. Cy., 21, GB1S90, doi:10.1029/2006GB002720, 2007.
Sigman, D. M., Altabet, M. A., McCorkle, D. C., François, R., and Fischer, G.: The δ^{15}N of nitrate in the Southern Ocean: Consumption of nitrate in surface waters, Global Biogeochem. Cy., 13, 1149–1166, 1999.
Sigman, D. M., Hain, M. P., and Haug, G. H.: The polar ocean and glacial cycles in atmospheric CO_2 concentration, Nature, 466, 47–55, doi:10.1038/nature09149, 2010.
Sloyan, B. M. and Rintoul, S. R.: Circulation, renewal, and modification of Antarctic mode and intermediate water, J. Phys. Oceanogr. 31, 1005–1030, 2001.
Smetackek, V., Assmy, P., and Henjes, J.: The role of grazing in structuring Southern Ocean

OSD
8, 639–674, 2011

pelagic ecosystems and biogeochemical cycles, Antarct. Sci., 16, 541–558, 2004.
Sokolov, S. and Rintoul, S. R.: On the relationship between fronts of the Antarctic Circumpolar Current and surface chlorophyll concentration in the Southern Ocean, J. Geophys. Res. 112, C07030, doi:10.1029/2006JC004072, 2007.
Sokolov, S. and Rintoul, S. R.: Circumpolar structure and distribution of the Antarctic Circumpolar fronts: 1. Mean circumpolar path, J. Geophys. Res., 114, C11018, doi:10.1029/2008JC005108, 2009.
Speich, S., Arhan, M., Gladyshev, S., Perrot, X., Fine, R., and Boyé, M.: Ocean structure and dynamics along BONUS-Goodhope, Ocean Sci. Discuss., in preparation, 2011.
Takeda, S.: Influence of iron availability on nutrient consumption ratio of diatoms in oceanic waters, Nature, 393, 774–777, 1998.
Toggweiler, J. R., Russell, J. L., and Carson, S. R.: Midlatitudes westerlies, atmospheric CO_2, and climate change during the ice ages, Paleoceanography, 21, PA2005, doi:10.1029/2005PA001154, 2006.
Tomczak, M. and Godfrey, J. S.: Regional Oceanography: An Introduction, Pergamon, New York, 2001.
Usbeck, R.: Modeling of marine biogeochemical cycles with an emphasis on vertical particle fluxes, Ph.D. thesis, 105 pp., Univ. Of Bremem, Bremen, Germany, 1999.
van Ballegooyen, R. C., Gründlingh, M. L., and Lutjeharms, J. R. E.: Eddy fluxes of heat and salt from the southwest Indian Ocean into the southeast Atlantic Ocean: A case study, J. Geophys. Res., 99(C7), 14053–14070, 1994.
Varela, D. E., Pride, C. J., and Brzezinski, M. A.: Biological fractionation of silicon isotopes in Southern Ocean surface waters, Global Biogeochem. Cy., 18, GB1047, doi:10.1029/2003GB002140, 2004.
Watson, A. J. and Naveira Garabato, A. C.: The role of Southern Ocean mixing and upwelling in glacial-interglacial atmospheric CO_2 change, Tellus, 58B, 73–87, 2006.
Young, E. D., Galy, H., and Nagahara, H.: Kinetic and equilibrium mass-dependent isotope fractionation laws in nature and their geochemical and cosmochemical significance, Geochim. Cosmochim. Ac., 66(6), 1095–1104, 2002.

OSD
8, 639–674, 2011

Table 1. $Si(OH)_4$ concentration and isotopic composition. Only the standard deviations for duplicates are shown. The solid lines represent the mixed layer depth.

Station	Depth m	$Si(OH)_4$ µmol l^{-1}	$\delta^{30}Si_{Si(OH)_4}$ ‰	sd ‰
Super 5	29	65.2	1.85	0.00
16 March 2008	88	64.2	2.00	
00.02° E–57.32° S	151	84.1	1.50	0.03
	199	96.2	1.35	0.01
	251	101.5	1.37	0.05
	299	104.2	1.41	0.05
	400	110.5	1.44	0.36
	499	117.2	1.47	
	700	116.5	1.44	0.20
	1003	120.0	1.27	
	1499	119.1	1.13	
	1999	116.6	1.12	0.06
	2500	119.7	1.43	
	3000	117.2	1.11	0.08
	3979	118.8	1.08	
Large 7	4	50.7	1.95	
14 March 2008	80	50.0	1.78	0.07
00.03° E–55.14° S	100	58.9	1.77	0.11
	149	74.4	1.54	
	199	79.7	1.53	0.17
	300	86.5	1.61	
	600	93.9	1.25	0.08
	1002	103.5	1.34	
	2096	122.7	1.38	
	2768	129.2	1.43	0.03
Super 4	11	22.2	2.42	
11 March 2008	79	22.3	2.37	0.06
00.00° E–51.87° S	100	21.9	2.16	0.08
	149	30.5	2.03	
	199	63.2	1.48	0.00
	300	86.0	1.41	0.09
	398	87.6	1.58	0.17
	553	88.9	1.37	0.16
	704	90.1	1.53	
	1201	101.9	1.35	
	1601	109.5	1.47	
	2001	121.6	1.30	
	2551	131.2	1.13	

OSD
8, 639–674, 2011

Table 1. Continued.

Station	Depth m	$Si(OH)_4$ µmol l^{-1}	$\delta^{30}Si_{Si(OH)_4}$ ‰	sd ‰
Large 6	3	4.0	2.47	
8 March 2008	48	4.0	2.48	
01.18° E–50.22° S	98	5.1	2.47	
	129	20.1	2.03	
	200	41.3	2.04	
	251	48.2	1.57	0.15
	401	64.4	1.42	0.13
	602	75.7	1.39	
	801	79.3	1.46	
	999	79.1	1.37	0.15
	1501	78.4	1.44	
	2002	93.1	1.28	
	2500	115.4	1.36	
	2998	124.7	1.38	
	3596	125.9	1.62	
Large 5	9	1.8	2.77	
7 March 2008	70	1.9	2.84	0.08
02.50° E–49.02° S	100	2.0	1.99	0.03
	151	7.2	2.07	
	200	13.8	1.92	
	300	22.4	1.36	
	402	30.9	1.99	0.28
	600	44.6	1.63	
	799	65.6	1.53	0.01
	1000	68.2	1.58	
	2001	76.2	1.41	
	3001	105.7	1.37	
	4080	128.6	1.44	
Super 3	5	2.1	3.24	0.01
6 March 2008	41	2.1	2.85	
04.23° E–47.33° S	79	2.2	2.36	
	100	4.2	2.57	0.19
	149	9.2	2.30	
	200	10.4	2.42	
	401	25.3	1.93	0.35
	600	42.5	1.67	
	1002	67.8	1.43	
	1403	70.0	1.42	
	2000	76.6	1.34	
	2301	85.6	1.26	0.01
	2900	101.8	1.39	0.34
	3500	116.0	1.16	
	4101	122.6	1.37	
	4532	132.1	1.28	

OSD
8, 639–674, 2011

Table 1. Continued.

Station	Depth m	$Si(OH)_4$ $\mu mol\,l^{-1}$	$\delta^{30}Si_{Si(OH)_4}$ ‰	sd ‰
Large 4	5	1.0	2.50	0.05
3 March 2008	32	1.2	3.01	
05.52° E–46.01° S	61	1.1	2.44	
	90	2.9	2.72	
	151	6.9	2.41	
	300	16.3	1.90	
	501	29.5	1.70	
	749	51.5	1.68	0.07
	1000	68.3	1.45	
	1502	75.4	1.51	
	1999	73.3	1.36	0.09
	2497	87.1	1.36	
	3001	104.4	1.43	
	3500	113.7	1.40	
	4148	126.0	1.47	
Large 3	11	1.0	2.46	0.19
2 March 2008	28	0.9	2.78	0.23
06.53° E–44.54° S	101	4.4	2.32	0.12
	149	6.0	2.07	
	298	11.1	2.06	
	400	14.8	1.83	0.10
	1251	66.8	1.54	
	1997	71.4	1.51	
	3001	95.8	1.36	
	3601	110.5	1.22	
	4371	125.9	1.24	
Super 2	10	0.6	3.24	0.05
27 February 2008	40	1.0		
08.56° E–42.28° S	80	2.5	2.07	0.06
	100	3.2	1.89	0.08
	150	4.8	2.09	
	300	9.5	2.01	0.14
	601	19.0	1.83	
	1001	46.9	1.50	0.1
	1400	68.0	1.29	0.11
	2000	71.6	1.28	
	2501	66.1	1.42	0.09
	3500	87.1	1.30	
	4057	110.6	1.36	

OSD
8, 639–674, 2011

Table 1. Continued.

Station	Depth m	$Si(OH)_4$ $\mu mol\,l^{-1}$	$\delta^{30}Si_{Si(OH)_4}$ ‰	sd ‰
Large 2	101	1.2	1.96	
21 February 2008	200	3.1	1.89	
13.10° E–36.45° S	504	14.4	1.77	
	600	18.9	1.73	
	1000	48.4	1.55	0.07
	2001	64.0	1.48	
	2900	69.2	1.57	
	4200	114.9	1.44	
	4570	117.9	1.13	0.01
Super 1	4	2.2	3.04	0.24
21 February 2008	25	2.3	2.89	0.07
13.10° E–36.45° S	75	4.5	2.07	0.01
	220	4.8	1.99	
	420	9.7	1.79	
	701	26.0	1.36	
	1002	51.4	1.64	
	1499	68.8	1.48	
	2001	60.0	1.37	
	2559	62.7	1.40	0.01
	2900	65.9	1.18	
	3499	88.2	1.51	
	4199	112.2	1.30	0.14
	4600	116.0	1.06	
	5000	115.6	1.05	

OSD
8, 639–674, 2011

Table 2. Average $Si(OH)_4$ concentrations and $\delta^{30}Si$ values for the different water masses defined during BONUS-GoodHope (±1 sd). ML: mixed layer, WW: winter water, AASW: Antarctic Surface Water, AAIW: Antarctic Intermediate Water, AZ: Antarctic Zone, PF: Antarctic Polar Front, PFZ: Polar Front Zone, SAF: SubAntarctic Front, SAZ: SubAntarctic Zone, STZ: Sub-Tropical Zone.

Water masses	$Si(OH)_4$ $\mu mol\,l^{-1} \pm sd$	$\delta^{30}Si_{Si(OH)_4}$ ‰ ± sd	*n*
AABW	121.0 ± 6.4	1.29 ± 0.16	21
LCDW	95.9 ± 18.9	1.36 ± 0.10	29
UCDW	71.9 ± 11.9	1.45 ± 0.10	24
AASW = WW (AZ-PF)	52.8 ± 22.5	1.58 ± 0.50	11
AAIW (PFZ-SAF-SAZ-STZ)	19.3 ± 14.6	1.93 ± 0.32	26
Thermocline (SAZ-STZ)	3.4 ± 1.3	1.99 ± 0.08	7
Summer ML (AZ)	36.2 ± 15.5	2.14 ± 0.27	5
Summer ML (PF)	4.4 ± 0.6	2.47 ± 0.01	3
Summer ML (PFZ)	2.0 ± 1.0	2.73 ± 0.29	9
Summer ML (SAF)	1.0 ± 0.1	2.62 ± 0.23	2
Summer ML (SAZ)	0.8 ± 0.3	3.24	2 – 1
Summer ML (STZ)	2.3 ± 0.1	2.96 ± 0.11	2

OSD
8, 639–674, 2011

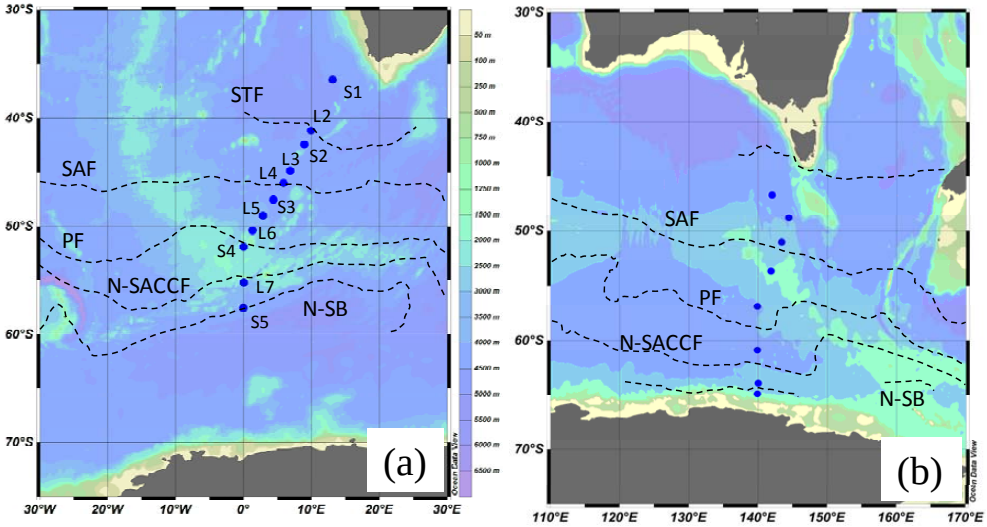

Fig. 1. Map of the BONUS-GoodHope (**a**; February–March 2007) and CLIVAR-SR3 (**b**; October–December 2001) sections with bathymetry and main hydrographic features (following Sokolov and Rintoul, 2009, and Swart et al., 2008; mean path position): STF = SubTropical Front; SAF = SubAntarctic Front (middle branch); PF = Polar Front (middle branch); N-SACCF = northern branch of the Southern ACC front; N-SB = northern branch of the Southern Boundary. The area north of the STF is called the SubTropical Zone (STZ), between STF and SAF the SubAntarctic Zone (SAZ), between the SAF and PF the Polar Front Zone (PFZ), between the PF and SB the Antarctic Zone (AZ), and south of the SB the Weddell Gyre (WG) in the left size and Seasonal Ice Zone in the right side. S refers to super stations and L to large stations. Mapping from R. Schlitzer (Ocean Data View, 2003, available at http://odv.awi.de/).

OSD
8, 639–674, 2011

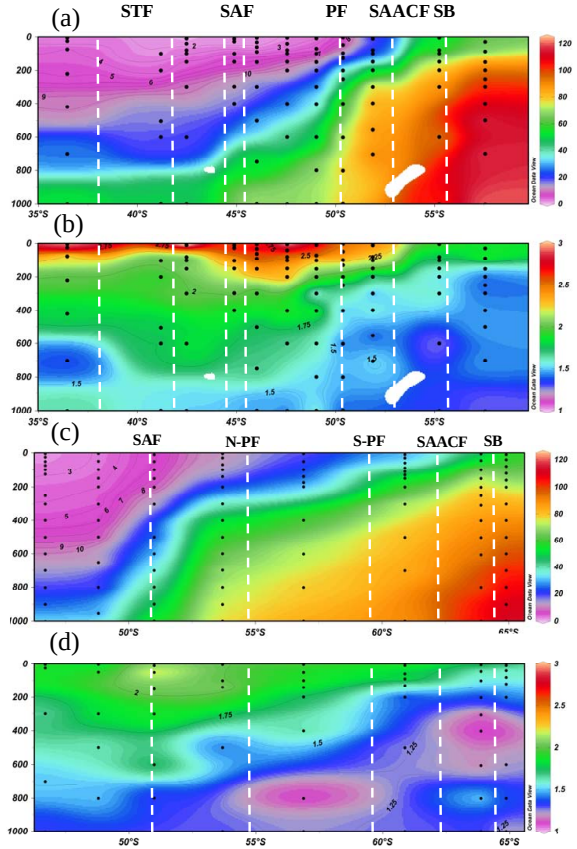

Fig. 2. Interpolation of δ^{30}Si (**b** and **d**) and [$Si(OH)_4$] (**a** and **c**) distributions in the upper 1000 m during BONUS-GoodHope (this study; **a** and **b**) and CLIVAR-SR3 (145° E; **(c)** and **(d)**, from Cardinal et al., 2005). Interpolation is from R. Schlitzer (Ocean Data View, 2003, available at http://odv.awi.de/). The position of the front at the time of sampling are also shown (dashed white lines).

OSD
8, 639–674, 2011

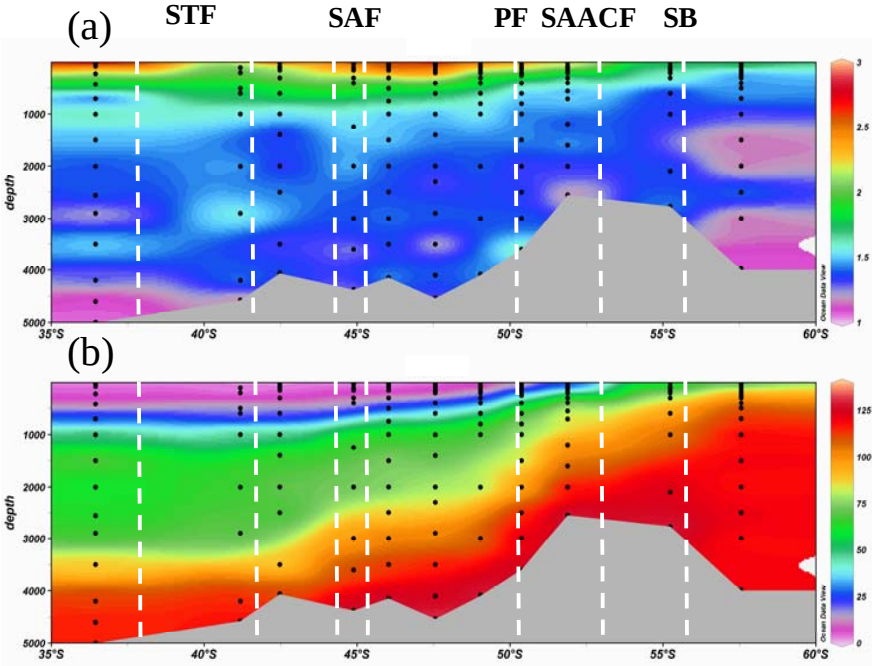

Fig. 3. Interpolation of δ^{30}Si **(a)** and [$Si(OH)_4$] **(b)** distributions for the complete water column during BONUS-GoodHope. Interpolation is from R. Schlitzer (Ocean Data View, 2003, available at http://odv.awi.de/). The position of the fronts at the time of sampling are shown as dashed white lines.

OSD
8, 639–674, 2011

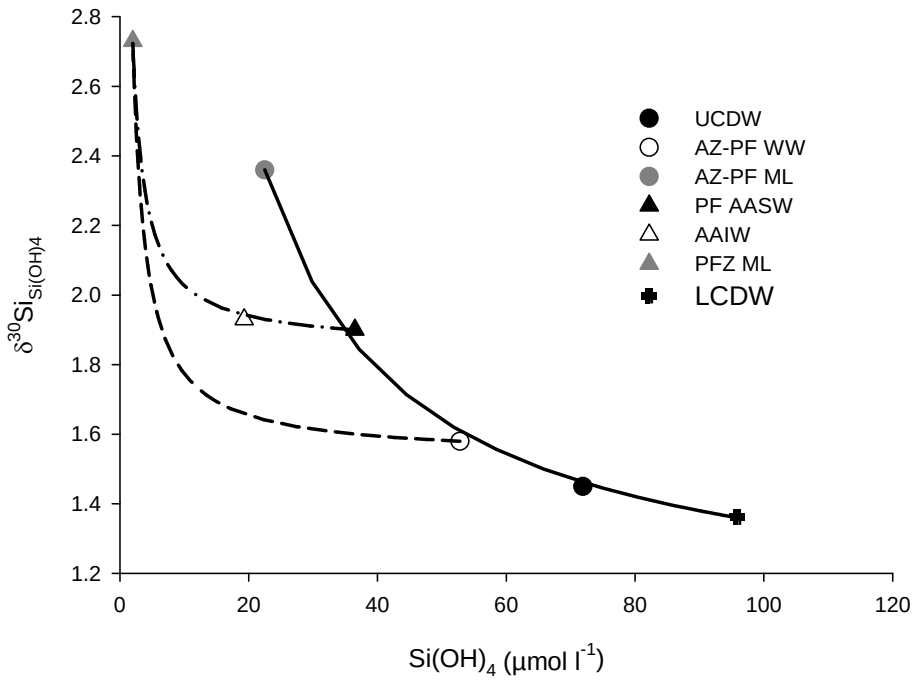

Fig. 4. The mean δ^{30}Si and Si concentration values for different water masses across the BONUS-GoodHope transect (this study). Some mixing lines are also shown: between LCDW and AZ-PF mixed layer (full black line), between PF-AZ AASW and PFZ mixed layer (dashed black line), and between PF AASW and PFZ mixed layer (dotted-dashed black line). When there is no indication of zone, it means that this is the average for the complete BGH transect.

OSD
8, 639–674, 2011

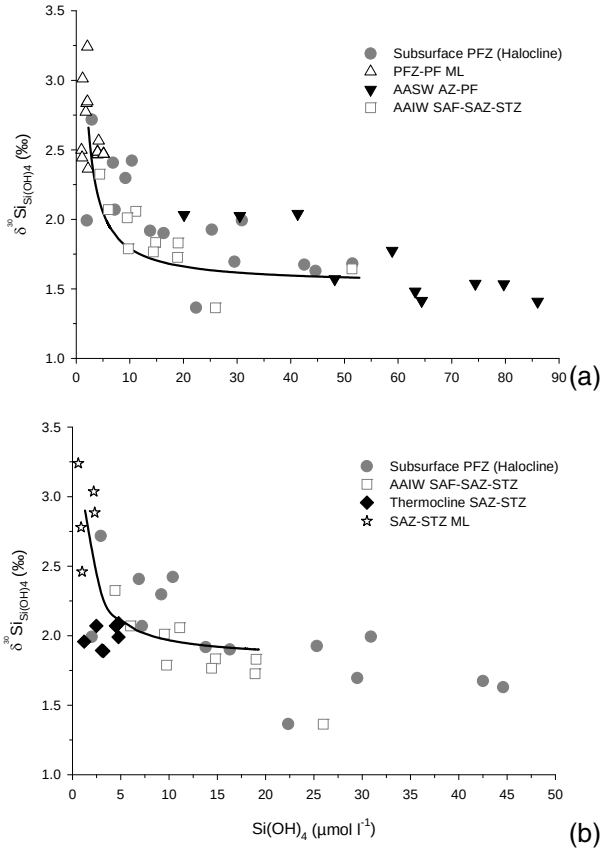

Fig. 5. **(a)** Mixing lines between AZ-PF WW and PFZ-PF ML (black line) with the average of some water masses in the AZ and PFZ. **(b)** Mixing line between STZ-SAZ mixed layer and AAIW. The end-members are estimated taking the average values for the considered water masses. When there is no indication of zone, the values shown reflect the distribution for the appropriate water masses across the complete BGH transect.

OSD
8, 639–674, 2011

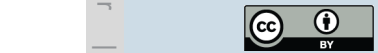

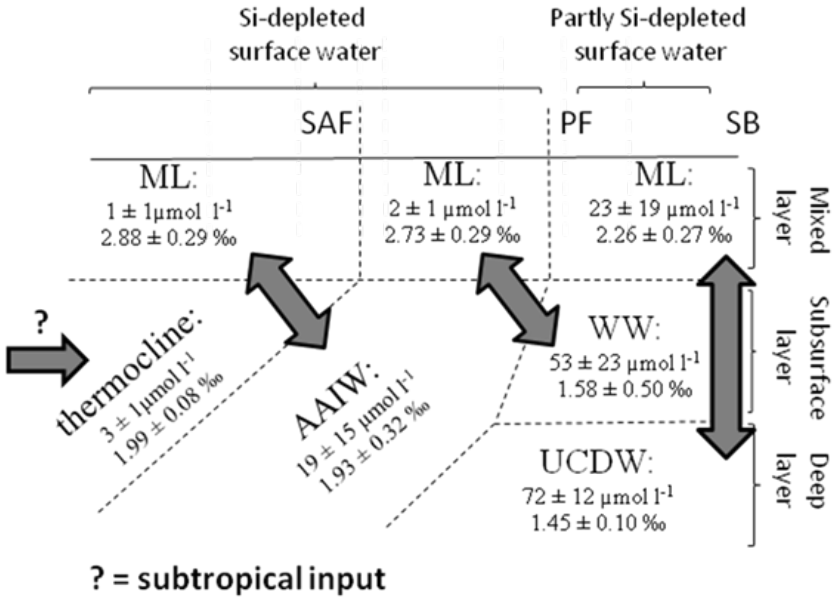

Fig. 6. Schematic view of the processes responsible for the observed δ^{30}Si distribution in subsurface waters, representing the mixing interfaces between surface and deeper waters. Identified mixing interfaces are the AASW = WW, the AAIW, and the low latitude thermoclines. The arrows represent the mixing end-members.

OSD
8, 639–674, 2011

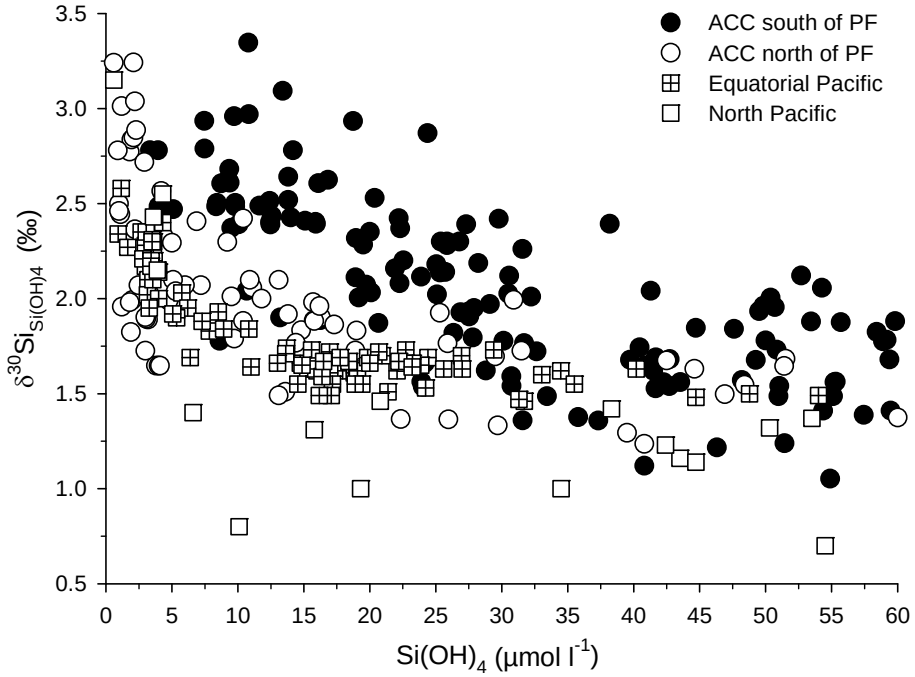

Fig. 7. δ^{30}Si vs. $Si(OH)_4$ for samples with Si <60 µmol Si l^{-1} in the ACC and the Pacific Ocean: ACC south of the PF are represented by black dots (Varela et al., 2004; Cardinal et al., 2005; Fripiat et al., 2011; Cavagna et al., 2011; this study), ACC north of the PF by white dots (Cardinal et al., 2005; this study), the Equatorial Pacific by crossed white squares (Beucher et al., 2008), and the north Pacific by white squares (De La Rocha et al., 2000; Reynolds et al., 2006).

OSD
8, 639–674, 2011

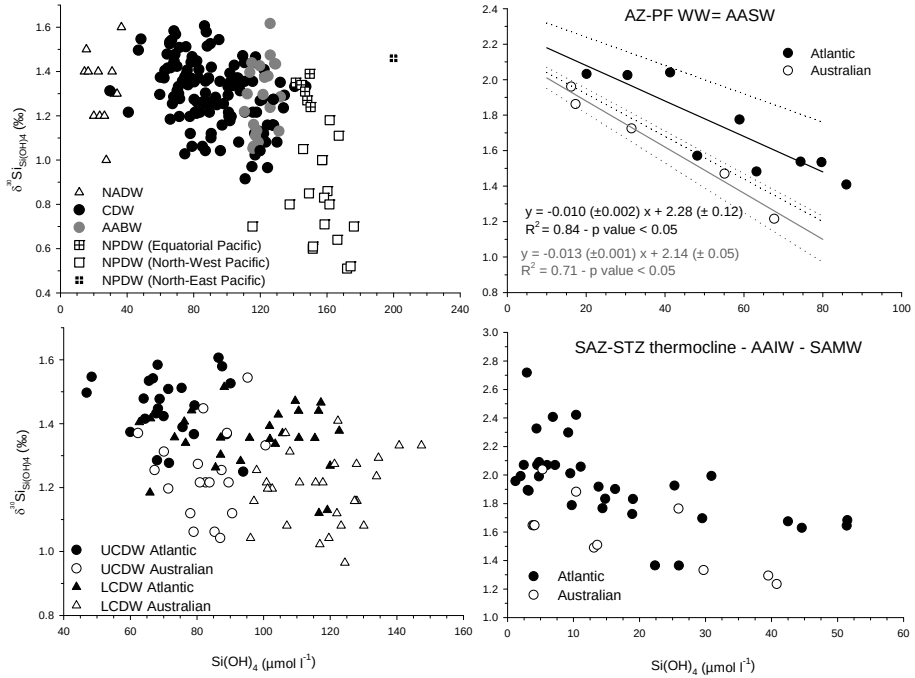

Fig. 8. (a) Deep water distribution in the different oceanic basins: NADW (De La Rocha et al., 2000), CDW (Cardinal et al., 2005; this study), AABW (Cardinal et al., 2005; this study), NPDW (De La Rocha et al., 2000; Reynolds et al., 2006; Beucher et al., 2008). **(b)** CDW distribution for the Atlantic and Australian sectors, respectively this study and Cardinal et al. (2005). **(c)** AZ-PF WW = AASW distribution for the Atlantic and Australian sectors, respectively this study and Cardinal et al. (2005). **(d)** SAZ-STZ thermoclines, AAIW, and SAMW for the Atlantic and Australian sectors, respectively this study and Cardinal et al. (2005).

OSD
8, 639–674, 2011